Mathematical Geology, Vol. 34, No. 3, April 2002 (© 2002)

First and Second Orders of Suture Complexity in Ammonites: A New Methodological Approach Using Fractal Analysis[1]

Juan A. Pérez-Claros,[2,4] Paul Palmqvist,[2] and Federico Olóriz[3]

The study of septal patterns in ammonoids has been centered on functional and/or constructional issues. Complexly fluted septa have been considered as complementary structures that reinforce the ammonite shell, their frilled sutures possibly manifesting the demand for strength. Ammonitic sutures display features that denote typical fractal behavior, since they can present very long perimeters relative to the contiguous shell areas, and most provide evidence of statistical self-similarity when observed at varying scales of magnification. However, there is a lower limit of scale measurements below which the fractal behavior of the curve no longer holds, and the perimeter length/step size relationship approaches an Euclidean geometry. This paper describes a new methodology that allows the accurate characterization of suture complexity in ammonoids using the technique of fractal analysis (step-line procedure). The proposed methodology helps to fix the position of this "cut-off point," allowing for independent estimates of the fractal dimensions of the curve for both large and small measurement scales (i.e., first and second orders of suture complexity). This approach improves the resolution of fractals in the analysis of suture complexity, thus facilitating the potential interpretation of suture patterns in functional/constructional, evolutionary and paleoecological terms.

KEY WORDS: Jurassic, ammonoids, morphometry.

INTRODUCTION

Chambered shells of cephalopods display some of the most beautiful designs in nature, but the functional interpretation of shell architecture and complex septal patterns of ammonoids has been a long-standing challenge. Most research in suture lines has dealt with evolutionary analyses based on systematics

[1]Received 2 August 2000; accepted 11 May 2001.

[2]Departamento de Geología y Ecología (Área de Paleontología), Facultad de Ciencias, Campus Universitario de Teatinos, 29071 Malaga, Spain; e-mail: johnny@uma.es; paul.palmqvist@uma.es

[3]Departamento de Estratigrafía y Paleontología, Facultad de Ciencias, Universidad de Granada, Campus de Fuentenueva, E-18002 Granada, Spain; e-mail: foloriz@goliat.ugr.es

[4]Present address: Geologish Paläontologishe Institut, Universität Heidelberg. Im Neuenheimer, Feld 234. D-69120 Heidelberg, Germany; e-mail: Juan.Perez@urz.uni-hd.de

(see overview in House and Senior, 1981), paleobiology (Boyajian and Lutz, 1992), and more recently paleoecology (Batt, 1991; Cecca, 1992; Daniel and others, 1997; Hewitt and Westermann, 1997). Covariance of suture complexity with other shell characters has also been investigated (Dommergues, Laurin, and Meister, 1996; Korn, 1992; Lutz and Boyajian, 1995; Olóriz and Palmqvist, 1995; Olóriz, Palmqvist, and Pérez-Claros, 1997, 1999; Saunders, 1995; Saunders and Work, 1996, 1997).

The functional significance of fluted septa and complex sutures in ammonoids has stirred debate during recent decades (Jacobs, 1996; Olóriz, Palmqvist, and Pérez-Claros, 1999). A persistent assumption has been that ammonoid shells were designed for resisting ambient hydrostatic pressure, frilled septa being interpreted as complementary structures of reinforcement of the phragmocone against hydrostatic pressure, and complex sutures as evidence of strength demands in shells inhabiting deep habitats (Buckland, 1836; Hewitt, 1993, 1996; Hewitt and Westermann, 1983, 1986, 1987, 1988a, 1988b, 1990, 1997; Jacobs, 1990; Pfaff, 1911; Westermann, 1971, 1973, 1975, 1977, 1982, 1985, 1996; Westermann and Ward, 1980). Other explanations arise from the fields of functional/constructional morphology, physiology, and developmental biology, including the buoyancy control (e.g., fluted septa resulting from inner gas-pressurization counteracting external water pressure, which allowed compression and decompression of a bladder by fleshy-membrane movability (Daniel and others, 1997; Kulicki, 1979; Kulicki and Mutvei, 1988; Saunders, 1995; Seilacher and LaBarbera, 1995; Ward, 1987), maximisation of the connective area of the mantle to the septum or number of muscular insertion points (Ebel, 1992; Henderson, 1984; Seilacher, 1975; Spath, 1919), transportation and storage of cameral fluid (Ward, 1980, 1987), and optimisation of phragmocone shell strength against the point loads such as the teeth of predators (Daniel and others, 1997). It has even been assigned a role in the respiratory process (Newell, 1949). Boyajian and Lutz (1992), in agreement with other authors (Fisher, 1986; Gould, 1988; Stanley, 1973), have suggested that the evolutionary trend of increase in suture complexity of ammonoids may be explained by dynamics of diffusion initiated by a simple condition expressing the generation of increasing variability. As the simplest form possible for a suture is a straight line, any increase in variability implies, intrinsically, an increase in maximum complexity.

Higher-order fluting was limited to the septum margin, resulting in increased suture complexity, and was accompanied by thinning of the septa; conversely, the center of strong septa was progressively thickened to compensate for stress concentrations (Hewitt, 1996; Westermann, 1975, 1996). Hewitt and Westermann (1997) have proposed that the main function of fluted septa was to buttress the wall of the inner septate whorls against an indirectly applied hydrostatic load. However, results obtained using a large database of Late Jurassic ammonites (Olóriz and Palmqvist, 1995; Olóriz, Palmqvist, and Pérez-Claros, 1997, 1999) revealed that suture complexity was similar in specimens inhabiting epicontinental shelves

and epioceanic plateaux, which suggests that suture complexity was not related to bathymetry and/or that there were no major differences in habitat depth for epicontinental and oceanic ammonites. Hence, deep habitats cannot be directly inferred from complex sutures, and direct measurements of radii of curvature and thickness of shell-wall, septa, and siphuncle are needed for calculating strength values and estimating paleobathymetry (Hewitt, 1996; Westermann, 1996). However, the analysis of biological structures in strictly physical terms provide estimations, which should be interpreted as potential rather than preferred ranges of function (Olóriz, Palmqvist, and Pérez-Claros, 1999).

The interpretation of the functional significance of complex sutures is clearly controversial and any research seeking to clarify the problem must answer two basic questions: (i) what is meant by suture complexity? and (ii) how can this characteristic be quantified? With respect to the first question, no precise definition has been made of the concept of complexity that can be applied universally, although many authors have attempted it, based on such disparate concepts as entropy, information, and fractal or grammatical complexity. McShea (1991) referred to a certain degree of consensus among researchers that morphologic or structural complexity, regardless of its relevance to biologic systems, can be considered a function of the number of parts and the irregularity of their order. The vagueness of this concept is, however, a serious hindrance to its application to real objects. It is, perhaps, more appropriate to tackle the problem another way, by responding instead to the second question, that is, by quantifying the spatial characteristics that are in some way related to complexity, and then relating the latter to the method utilized to characterize it.

With particular regard to the study of ammonoid sutures, the mathematical characterization of suture complexity has traditionally been performed using simple parameters. These include the index of suture complexity as first presented by Westerman (1971) and later termed *SCI* by Ward (1980) or *SI* by Saunders (1995). This is the quotient of the suture perimeter and the length of the segment joining the two extremities. This index has been applied in both basic and modified forms, the latter including the count of suture elements (Saunders, 1995). Canfield and Anstey (1981) attempted a mathematical description of sutures using Fourier series, although Lutz and Boyajian (1995) have observed that this methodology provides relatively little information on certain suture characteristics, such as the size distribution of lobes and saddles, and only enables relatively simple suture lines to be characterized.

Another way to quantify the degree of complexity is based on the use of fractal logic, by which the structure is considered to be self-similar for the observation scales being used. This characteristic is also known as internal homothety or self-similarity. A fractal object can be defined as a set comprised of parts that in one or more aspects are similar to the whole (Mandelbrot, 1984). This definition may be clarified with addition of two basic concepts: homothety and cascade. Homothety is an equiform transform in which the angles, and thus the shape of

the figure, remain unchanged. A more flexible view of this concept allows for the displacement and/or rotation of the points that make up the original figure. Repetition of the process ad infinitum (the process Mandelbrot termed "cascade") produces a fractal object. Figure 1 shows how a straight segment, the initiator, is

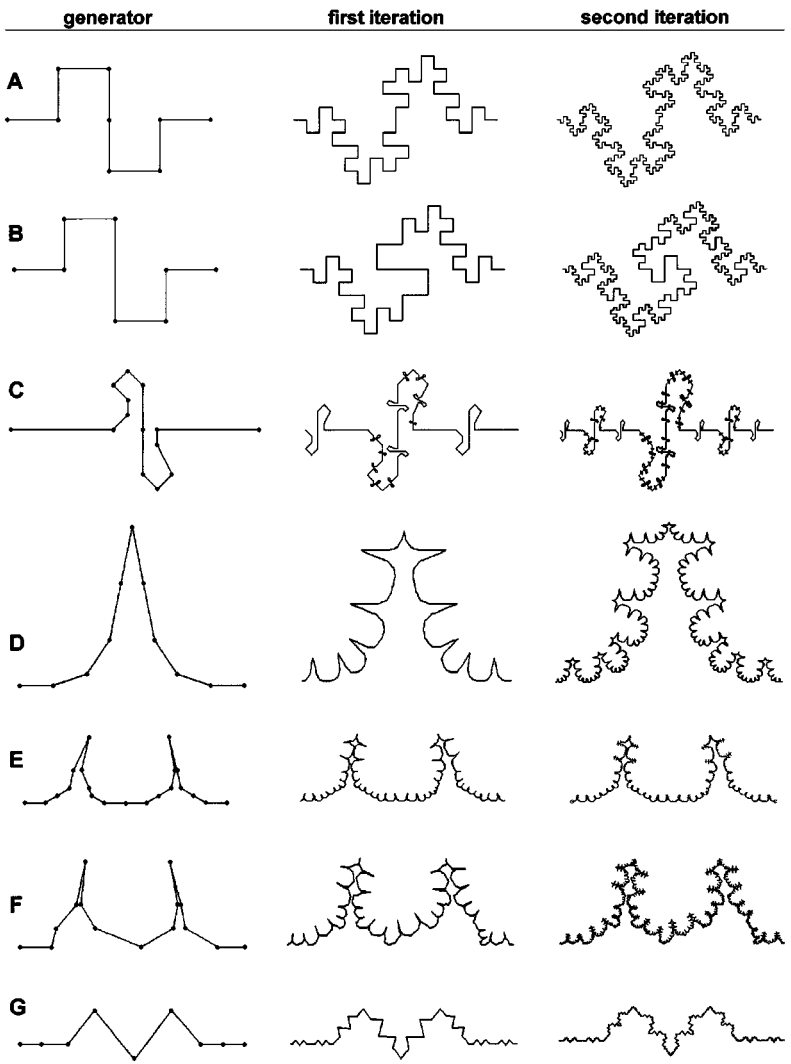

Figure 1. Various mathematical fractals, showing the shape of the generator (left-hand column) and the morphology of the curve after the first and second iterations (middle and right-hand columns, respectively).

transformed homothetically by a generator rule made up of parts which, in turn, are straight-line segments. When the original segment has been transformed, the procedure is repeated, with each of the resulting segments transformed in turn. Each segment generated by a transformation acts as the initiator of the following one. The result is the generation of a fractal figure that presents self-similarity. In Figure 1, each of the forms generated is identical to the original except in position and size. This type of object is called a perfect fractal, of exact or mathematical self-similarity. The degree of irregularity of each part is identical to that of the whole. In general, natural objects in which some kind of internal homothety can be detected (such as ammonitic sutures) are far from meeting the rigorous definition of a perfect fractal. Nevertheless, the degree of abruptness, irregularity, or sinuosity of the regions into which such objects can be divided is approximately the same. These objects are therefore described as fractals of statistical self-similarity (i.e., the exact shape of the object is not maintained when the observation scale changes, but the degree of complexity is).

Various authors have described the self-similar nature of ammonoid suture lines (Bayer, 1985; Damiani, 1986; Seilacher, 1988). The first specific reference to the term fractal (with all its connotations) was Long (1985). Although he did not examine the topic in detail, he described the statistical self-similarity of the curves and estimated the value of some fractal exponents. Lutz and Boyajian (1995) explicitly concluded that ammonitic sutures comprise the necessary characteristics for self-similarity, although in goniatites and ceratites this condition is more doubtful because they are self-similar over a shorter range of scale measurements (for cranial sutures, see Long and Long, 1992).

One of the most important properties of fractals resides in their fractal dimension (D_f), which is a measure of their degree of irregularity or sinuosity. This measure is closely related to the effective physical dimension (D_e), which is the degree to which the object being analyzed presents a topological (i.e., Euclidean) dimension with a value equal to or greater than what it should theoretically present. This concept is exemplified by the leafy top of a tree that has a mass of plane structures ($D_e = 2$), even though the manner in which they are organized almost fills a volume ($D_e = 3$). Similarly, the projection in a plane of the Brownian movement of a particle, recorded at regular time intervals, describes such a complicated trajectory that it is only perceived as a tangled mass that occupies virtually the entire plane ($D_e = 2$), even though it is actually made up of straight lines ($D_e = 1$). In the first example, the effective physical dimension that best describes the figure would be somewhere between 2 and 3, while in the second one it would be almost equal to 2. In general terms, the physical dimension that best reflects this kind of figure is the fractal dimension, which need not be an integer. The purpose of fractal analysis is to determine the fractal dimension of figures or processes that present some type of internal homothety.

García-Ruíz, Checa, and Rivas (1990) attempted to characterize ammonite suture complexity using the fractal dimension as a mathematical descriptor.

Throughout ontogenetic sequences, this magnitude was related to a morphogenetic model to form septal patterns, based on the instabilities occurring when two fluids mix in a nonuniform way as dictated by the distinct viscosity of the compressed mantle and the cameral fluid in the last chamber. In their viscous fingering model, García-Ruíz, Checa, and Rivas (1990) proposed that ammonite sutures were the result of a morphogenetic process containing a Saffman-Taylor-type instability. Boyajian and Lutz (1992) applied fractal analysis to quantify the evolution of suture complexity among ammonoids as a whole, virtually from their first appearance to their eventual extinction. To achieve this, they examined the sutures of 615 genera belonging to seven different orders. They also studied the relation between suture complexity and the stratigraphic range of the genera analyzed, as an estimator of their evolutionary longevity. They did not find the inverse relation between the two parameters that, a priori, was to be expected (assuming that suture complexity does in fact allow the estimation of degree of specialization in evolutionary lines). Subsequently, Lutz and Boyajian (1995) studied the efficacy of various suture complexity estimation methods, such as interrelation between the fractal analysis parameters among ceratitic, goniatitic, and ammonitic sutures, the three main suture types into which ammonoid sutures are normally grouped. Olóriz and Palmqvist (1995) and Olóriz, Palmqvist, and Pérez-Claros (1997, 1999) studied the relationships between various morphologic and paleoecologic categories and the fractal dimension, for a geographically widespread group of ammonites from the Late Jurassic ($N = 507$). They found a range of D_f estimates (1.185–1.661) wider than those provided by previous researchers, and showed that epioceanic ammonoids (which were presumably capable of living in a large range of water depths) have D_f values that are similar to those of epicontinental taxa. Suture complexity was more closely related to the size, geometry, and hydrodynamic properties of the shell; for example, involute phragmocones with subtriangular or very high ovate whorl-sections provide the highest fractal dimension values ($D_f > 1.5$), these morphologies corresponding to potentially more active swimmers, with improved steerage (i.e., maneuverability combined with directional stability) and relative speed during the pursuit of prey (Olóriz, Palmqvist, and Pérez-Claros, in press).

These studies assume the self-similarity of the suture at various scales. Nevertheless, for any natural object there exists a lower and a higher observation scale, termed "inner cut-off" and "outer cut-off," respectively, by Mandelbrot (1984), beyond which the object lacks self-similarity and thus does not behave as a fractal (i.e., the curve does not provide a double-log plot of negative slope). To date, these limits have been determined by visual means (Boyajian and Lutz, 1992; Long, 1985; Long and Long, 1992; Lutz and Boyajian, 1995; Olóriz and Palmqvist, 1995; Olóriz, Palmqvist, and Pérez-Claros, 1997, 1999).

In this paper we present a new method to achieve the fractal characterization of sutures, which enables us to identify two important characteristics of fractal

objects: (i) their fractal dimension, as a morphometric descriptor of the tendency of the suture to coat a surface; and (ii) the degree of self-similarity, restricted to the lower scales or "inner cut-offs," beyond which the self-similar quality is lost. By considering these two characteristics separately, a more efficient analysis of suture complexity is achieved. This is because an increase in both the fractal dimension and the degree of self-similarity of a structure lead to an increase in the complexity of the latter, as can be confirmed visually.

The method we present is limited to connected fractal curves with D_f values between 1 and 2, and was tested on ammonitic sutures, which provide an excellent example of statistically self-similar fractals over a wide range of scale measurements. Goniatitic and ceratitic sutures were discarded from this study because they display a short range of scaling and self-similarity (Lutz and Boyajian, 1995). This basic method can, in turn, be applied to other types of fractal curves that fulfil the above requirement.

METHOD

The proposed methodology was developed for exactly self-similar fractals, because they allow a priori determination of (i) the theoretical value of the fractal dimension; and (ii) the size of each part of the curve in relation to the whole, for different levels of iteration, when a cascade mechanism is used to generate the curve.

In the case of perfect connected fractal figures with identical homothety ratios, where D_f is between 1 and 2 (e.g., Fig. 1(A)), the value of D_f can be obtained from the following equation:

$$N = r^{-Df}, \tag{1}$$

where N is the number of parts (i.e., the number of segments comprising the generator, eight in Fig. 1(A)) and r is the homothety ratio of each part (i.e., the ratio between the size of each part and that of the initiator, 1/4 in this case). In more general terms, when the homothety ratios are not identical, as is the case in Figure 1(B), the value of D_f can be estimated by the following equation:

$$\sum_{i=1}^{N} r_i{}^{Df} = 1,$$

where i is the ith part into which the generator can be decomposed.

Note that if the shape of the generator of a fractal figure is not known a priori, it is not possible to obtain the homothety ratios generated by successive

parts. Moreover, in the general case of statistically self-similar fractals there is no generator that is exactly repeated in successive iterations. There are various methods to determine D_f in these cases, of which the best known is Richardson's (Richardson, 1961) (Fig. 2). This consists of estimating the perimeter of the figure for different arbitrary rule sizes (λ). The curve length (L_e) is calculated for each rule size (λ), multiplying λ by the number of times this rule fits in the figure (i.e., $N_{(\lambda)}$). Thus the homothety ratios are defined by

$$r\left[N_{(\lambda)}\right] = \frac{\lambda}{L_{\max}},$$

where $L_{\max}$ corresponds to the initiator length (unknown in this case); statistically, the following equation is fulfilled:

$$N_{(\lambda)} = r\left[N_{(\lambda)}\right]^{-D_f}.$$

Therefore,

$$L_e = N_{(\lambda)}\lambda = r\left[N_{(\lambda)}\right]^{-D_f\lambda} = \left(\frac{\lambda}{L_{\max}}\right)^{-D_f\lambda},$$

$$\log(L_e) = \log\left(\frac{\lambda^{(1-D_f)}}{{L_{\max}}^{-D_f}}\right),$$

which is equivalent to

$$\log(L_e) = D_f\ \log(L_{\max}) + (1 - D_f)\ \log(\lambda) = n + m\log(\lambda) \qquad (2)$$

Thus, taking the logarithm of the estimated length of the fractal curve [$\log(L_e)$] as a function of the logarithms of the different sizes for the corresponding rules [$\log(\lambda)$], D_f and the value of the parameter $L_{\max}$ can be determined by fitting the cluster of points to a straight line, where

$$D_f = 1 - m; \qquad L_{\max} = \exp\left(\frac{n}{D_f}\right).$$

Equation (2) is valid for both exact and statistically self-similar fractals, such as ammonite sutures (Fig. 3), although it assumes the figure behaves as a fractal object to an indefinitely small size.

In general, fractal objects found in nature (as well as computer-simulated ones) present a lower scale boundary or inner cut-off, below which they are no longer self-similar replicas and cease to behave as fractals. In these cases, it is

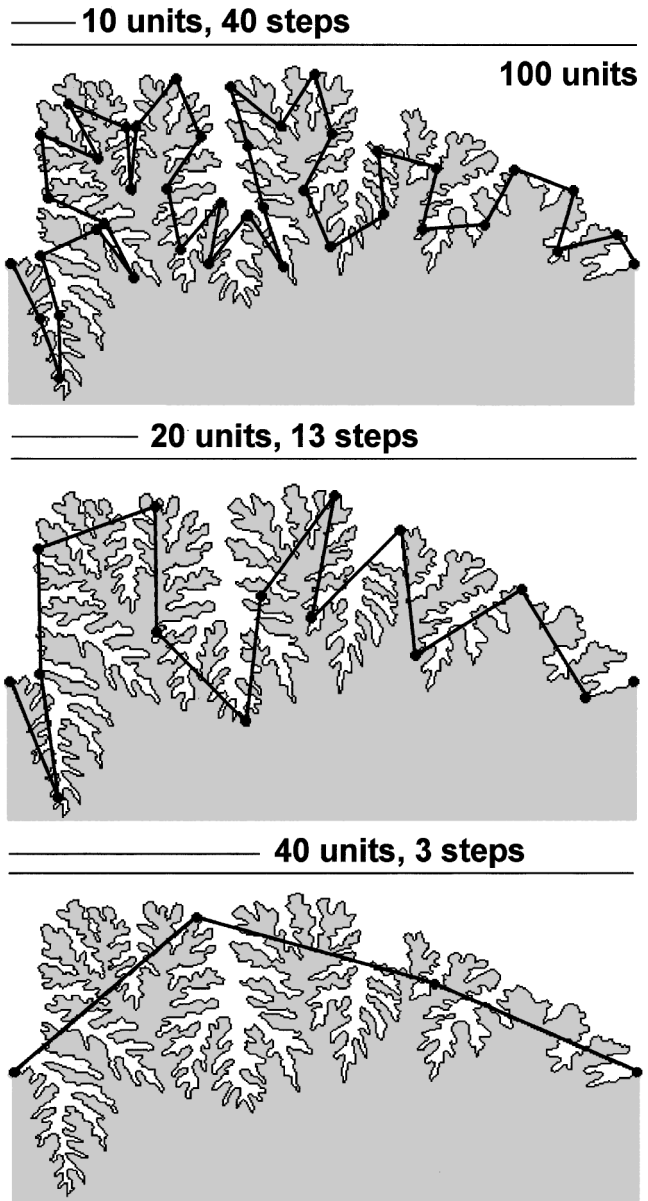

Figure 2. Richardson's method, or compass method, to estimate the mean fractal dimension (D_f) for an ammonitic suture.

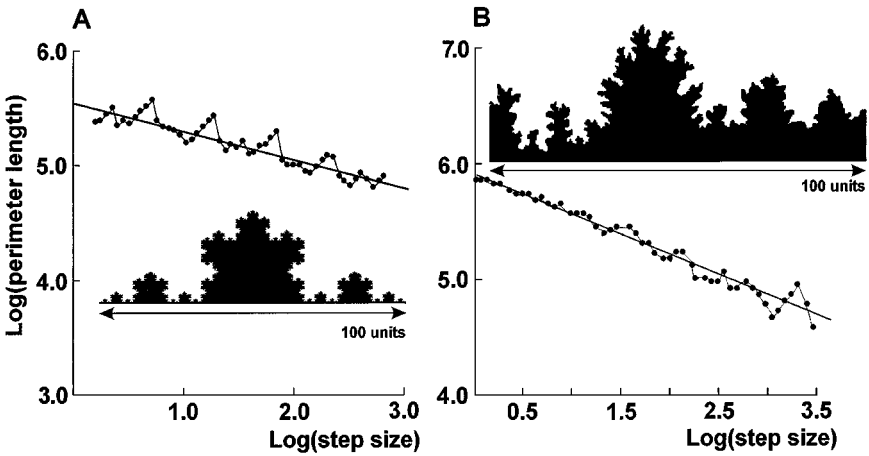

Figure 3. Bilogarithmic representation to estimate the mean fractal dimension (D_f) in (A) a perfect mathematical fractal curve (von Koch's curve) and (B) a statistically self-similar fractal curve (ammonitic suture), obtained by the inverse relation between the rule length or measurement scale and the perimeter of the curve estimated with this rule. The curves were standardized to a linear length of 100 units.

more appropriate to describe the objects at their smallest scale by Euclidean geometry. Thus, if we measure the curve with rules smaller than the self-similarity inner cut-off, the bilogarithmic representation diverges from a negative-sloped straight line, as this limit becomes increasingly distant and approaches an asymptotic trajectory with a horizontal component (Fig. 4(A) and (B)). In such cases, it is standard practice to eliminate from the regression adjustment the points that do not coincide with the theoretical slope obtained with an ad infinitum fractal object (Lutz and Boyajian, 1995; Olóriz, Palmqvist, and Pérez-Claros, 1997, 1999).

The proposed method, on the other hand, enables the establishment of a rule-length value (arbitrary, but objective) that determines an inner cut-off that is fully comparable between different fractal figures. The method is valid only if such parameters are standardized at a fixed distance between two equivalent points that are sampled with the same rule lengths. This condition is satisfied in ammonitic sutures at the mid-point of the ventral saddle and the flank point where the suture is no longer visible due to the curvature of the shell. Thus, Figure 4(A) and (B) can be idealized as in Figure 4(C), where there is a final region that represents the typical features of fractal objects. As the rule lengths diminish the curve approaches a null slope and the value of the fractal dimension in this region approaches that of the Euclidean or topologic dimension (i.e., 1, for a straight line).

In this case, if the maximum rule length analyzed (X_f) is arbitrarily determined such that it is small in relation to the value of L_{max}, the bilogarithmic representation

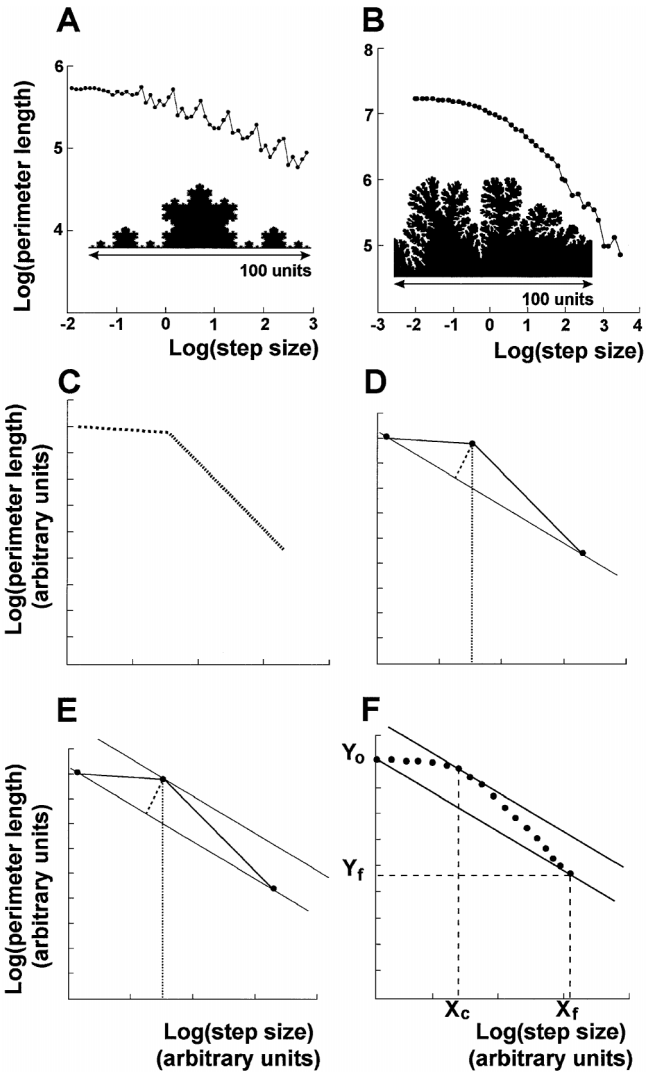

Figure 4. Change in slope in the relation between the estimated perimeter for a fractal curve (A) and the ammonitic suture of *Holcostephanus* (*Spiticeras*) *scriptus* (B), in relation to the rule size used. This change is related to the loss of fractal behaviour below a limit value of the measurement scale (X_c), beyond which there is a transition to Euclidean geometry. The proposed method to establish the cut-off point is illustrated (see text for details).

can be considered to consist of two regions, described by two independent curves (Fig. 4(D)). Therefore, if the scale at which the transition between the two series of rule lengths is characterized, it is possible to fit the two components of the representation to straight lines. To determine the value of the transition or cut-off point (X_c) between the two regions, a simple model can be used. The model dictates that if the initial bilogarithmic representation comprised two curves with different slopes, the transition point occurs where the curve is most distant from the line joining the two ends of the representation (Fig. 4(E)). If the two linear trends of the bilogarithmic representation are integrated into a new, single function (derivable at all scales analyzed), the criterion to determine the value of X_c consists of finding the point where the derivate of the function corresponds to the slope of the curve joining the two ends of the above function (Fig. 4(F)). The function to which the bilogarithmic representation can be fitted, first to determine the value of X_c and then to fit the least squares regression, is defined by adapting the following allometric model:

$$\log(L_e) = K - a[\log(\lambda)]^b = y^* = K - ax^b. \quad (3)$$

In these circumstances, the value of K can be approximated by the observed value of $\log(L_e)$, which corresponds to the smallest rule length analyzed, while a and b can be calculated by a nonlinear adjustment. This provides more accurate estimates than those obtained from the logarithmic linearization of Equation (3).

The pairs of values thus obtained ($y = y^* - K$) are fitted to the following curve:

$$y = -ax^b,$$

which now cuts both axes at point (0,0).

After estimating the values of a and b the specific expression of their derivates is calculated

$$y = -abx^{b-1}.$$

The slope of the line joining the two ends of the curve is calculated by

$$mt = \frac{(Y_f - Y_0)}{(X_f - X_0)},$$

which is equivalent to

$$mt = \frac{Y_f}{X_f},$$

because the first of these two ends is the origin.

Given that the value of X_f can be established as a constant, the whole function can be expressed as follows:

$$mt = \frac{-aX_f{}^b}{X_f} = -aX_f{}^{b-1}.$$

The criterion for finding the value of X_c can therefore be expressed unequivocally as the value of x in which the derivative of the function at that point is equal to mt:

$$-a\ X_f{}^{b-1} = -ab\ X_c{}^{b-1}.$$

From the above equation, we obtain

$$X_c = \frac{X_f}{b^{(1/b-1)}},$$

which proves that the value of X_c does not depend on the value of a. In this expression, X_c is obtained as a proportion of X_f, that, in turn, is a characteristic of all fitted bilogarithmic slopes.

If the fractal character of the curve is maintained at all scales, such that b tends to a value of 1, then the value of X_c at the limit is

$$\begin{aligned}\lim_{b\to 1^+} X_f/b^{(1/b-1)} &= X_f \lim_{b\to 1^+} b^{(1/b-1)} = X_f\ \exp\left[\log\left\{\lim_{b\to 1^+} b^{(1/b-1)}\right\}\right] \\ &= X_f\ \exp \lim_{b\to 1^+} [\log(b)/(1-b)],\end{aligned}$$

where

$$\lim_{b\to 1^+} \log(b)/(1-b) = \overset{\text{LiH}}{\lim_{b\to 1^+}} (1/b)/-1 = -1.$$

Therefore

$$X_f\ \exp[\lim_{b\to 1^+}\ \ln(b)/(1-b)] = X_f\ \exp(-1) = X_f/e.$$

When X_c has been determined, the bilogarithmic representation is characterized by two regions: one that presents a truly fractal nature, and another that tends to lose this fractal nature. X_c can be taken as an inverse index of self-similarity that is fully comparable between different fractal figures if these are analyzed with equivalent rule lengths. When a fractal figure can be identified unequivocally between two homologous points (as is the case with ammonitic sutures), the equivalence of the rule lengths or step sizes is established by standardizing

the figures to the same linear dimensions and analyzing them using the same rule lengths.

MATERIAL ANALYZED

To estimate the validity of the above model, it was first applied to a group of exactly self-similar fractal curves, which provided a controlled environment in which to test the proposed methodology. Subsequently, the model was applied to a diverse group of ammonitic sutures, thus enabling us to test whether the characteristics forecast by the model fitted what could be observed in a visual, intuitive way.

A group of exact fractal curves (with a D_f between 1.18 and 1.59) were used, each constructed with two iterations. The fractal curves and ammonitic sutures analyzed were standardized to a rule length of 100 arbitrary units from one end to another, using the Bookstein (1991) shape coordinates method:

$$x'_i = 100[(x_f - x_0)(x_i - x_0) + (y_f - y_0)(y_i - y_0)]/[(x_f - x_0)^2 + (y_i - y_0)^2],$$
$$y'_i = 100[(x_f - x_0)(y_i - y_0) - (y_f - y_0)(x_i - x_0)]/[(x_f - x_0)^2 + (y_i - y_0)^2],$$

where (x_i, y_i) are the Cartesian coordinates of the original points among which each suture was digitized, (x'_i, y'_i) are the shape coordinates estimated from the above, and (x_0, y_0) and (x_f, y_f) are the coordinates of the starting and finishing points of the original suture, respectively, which after transformation take the values (0, 0) and (100, 0).

The Richardson's method (Mandelbrot, 1984; Richardson, 1961) was used to obtain the bilogarithmic representation, running on 40 step sizes or rule lengths distributed in increasing base 2 powers, from 2^{-3} to $2^5[X_f = \log(32)]$, with exponential increments of 0.2. The count of the number of rules that can be included in each figure proceeds from left to right. When at least half of the last rule does not fit exactly into the last segment considered, this rule is not taken into consideration.

RESULTS AND CONCLUSIONS

Table 1 shows the fractal dimensions obtained for the curves analyzed at large- and small-scales (D_{f2} and D_{f1}, respectively), the theoretical fractal dimensions, assuming self-similarity ad infinitum (D_{ft}), the fractal dimension obtained without distinguishing the two series of scales (D_f), and the rule length for the transition between the two regions (X_c). It also shows the minimum, maximum, and mean lengths of the parts or segments comprising each of the figures. Note that the sizes of these parts can be specified in these cases, because the shape of the generators and

Table 1. Fractal Dimensions at Large (D_{f2}) and Small (D_{f1}) Scales for Various Mathematical Fractals (Fig. 1), Together With Values of the Theoretical ($D_{ft}/D_f^{theor.}$) and Mean (D_f) Fractal Dimensions, the Cut-Off Point (X_c), and the Minimum, Mean, and Maximum Sizes of the Segments That Comprise the Curves After Two Iterations

Generator	D_f theoretical	D_f	D_{f1}	D_{f2}	X_c	Min. distance	Mean distance	Max. distance
A	1.500	1.328	1.127	1.540	0.897	1.563	1.563	1.563
B	1.585	1.290	1.100	1.534	0.961	1.563	2.332	12.500
C	1.424	1.341	1.191	1.490	0.583	0.022	0.346	7.505
D	1.440	1.285	1.112	1.444	0.799	0.339	0.799	1.663
E	1.312	1.313	1.259	1.337	0.196	0.019	0.190	0.997
F	1.413	1.383	1.294	1.398	0.246	0.063	0.354	1.068
G	1.180	1.175	1.131	1.207	0.303	0.095	0.483	2.138

the number of iterations are known a priori; in statistically self-similar fractals, this cannot be established, but as the results of the fractal analysis only depend on the shape of the figure being analyzed and not on the number of points that comprise the segments, the results obtained in this study for the curves with exact self-similarity are fully comparable with those supplied by statistical fractals. Table 2 shows the values of the correlation coefficients between the variables obtained (lower triangular matrix) and the level of significance (upper triangular matrix).

Table 1 shows that the estimation of D_f that is closest to the theoretical fractal dimension is provided by D_{f2}, which is corroborated by the strong correlation of D_{f2} with D_f (Table 2). It is also noteworthy that D_{f2} is independent of the degree of self-similarity of the figure, and thus does not correlate significantly with X_c or with the maximum, minimum, or mean sizes of the parts that make up the figures. On the other hand both D_f and D_{f1} correlate well with these variables. The high, positive correlations between the logarithms of the sizes of the segments or parts that comprise the figures (minimum, maximum, and, above all, the mean) and

Table 2. Pearson Correlations Between the Parameters of Fractal Analysis (r, lower triangular matrix) and Their Level of Statistical Significance (p, upper triangular matrix)

$r_{Pearson}/p$	D_f theoretical	D_f	D_{f1}	D_{f2}	X_c	$\log(D_{min})$	$\log(D_{max})$	$\log(D_{mean})$
$D_f$theor.		0.013	0.434	<0.001	0.181	0.399	0.207	0.592
D_f	0.435		<0.001	<0.001	<0.001	0.001	<0.001	<0.001
D_{f1}	0.143	0.894		0.109	<0.001	<0.001	<0.001	<0.001
D_{f2}	0.859	0.621	0.289		0.614	0.627	0.992	0.432
X_c	0.243	−0.697	−0.851	0.093		<0.001	<0.001	<0.001
$\log(D_{min})$	0.155	−0.556	−0.634	−0.089	0.651		0.021	<0.001
$\log(D_{max})$	0.229	−0.594	−0.724	0.002	0.785	0.408		<0.001
$\log(D_{mean})$	0.099	−0.788	−0.885	−0.144	0.918	0.813	0.775	

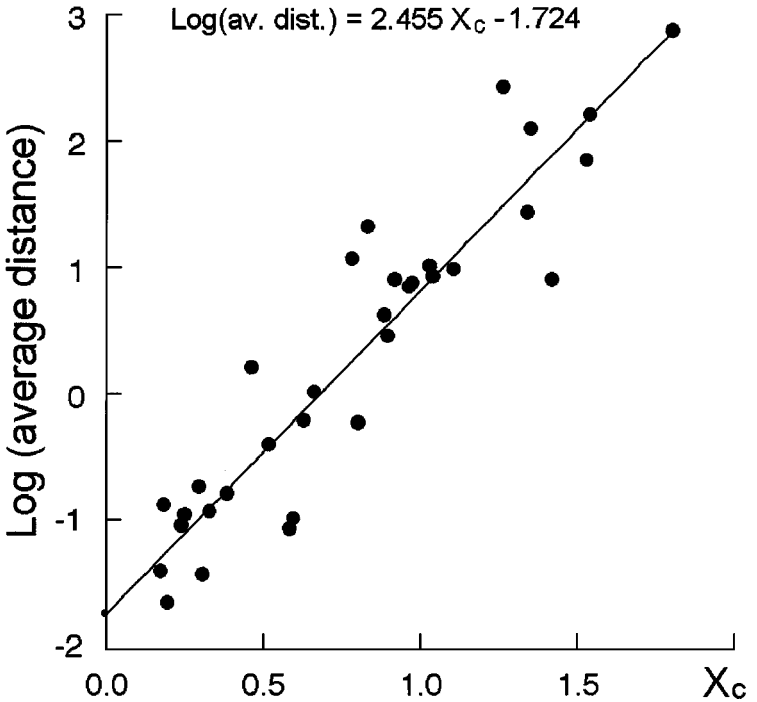

Figure 5. Direct relation between the mean size of the linear segments that comprise the fractal curves and the position of the cut-off point (X_c). In these segments, the relation between the calculated perimeter and the measurement rule follows Euclidean logic, with a null slope.

X_c (Fig. 5) indicate that the latter can be considered an effective inverse index of self-similarity.

When the above methodology is applied to the analysis of real sutures (Table 3 and Fig. 6), the effectiveness of the method is apparent. For example, both Figure 6(A) and (E) show striking differences between the absolute fractal

Table 3. Parameters of Fractal Analysis for the Sutures Shown in Figure 5

Figure	Species	*a*	*b*	*K*	X_c	D_{f1}	D_{f2}
5A	*Hoplites (Blandfordia) curvatus*	0.439	1.228	6.852	1.416	1.468	1.674
5B	*Pseudolisoceras zitteli*	0.308	1.096	5.864	1.339	1.327	1.361
5C	*Taramelliceras callicerum*	0.176	1.725	6.575	1.601	1.250	1.607
5D	*Holcostephanus (Spiticeras) scriptus*	0.376	1.371	7.023	1.465	1.414	1.731
5E	*Oppellia (Streblites) indoptica*	0.229	1.774	7.185	1.627	1.358	1.886
5F	*Glochiceras nimbatum*	0.042	2.066	5.176	1.811	1.058	1.231

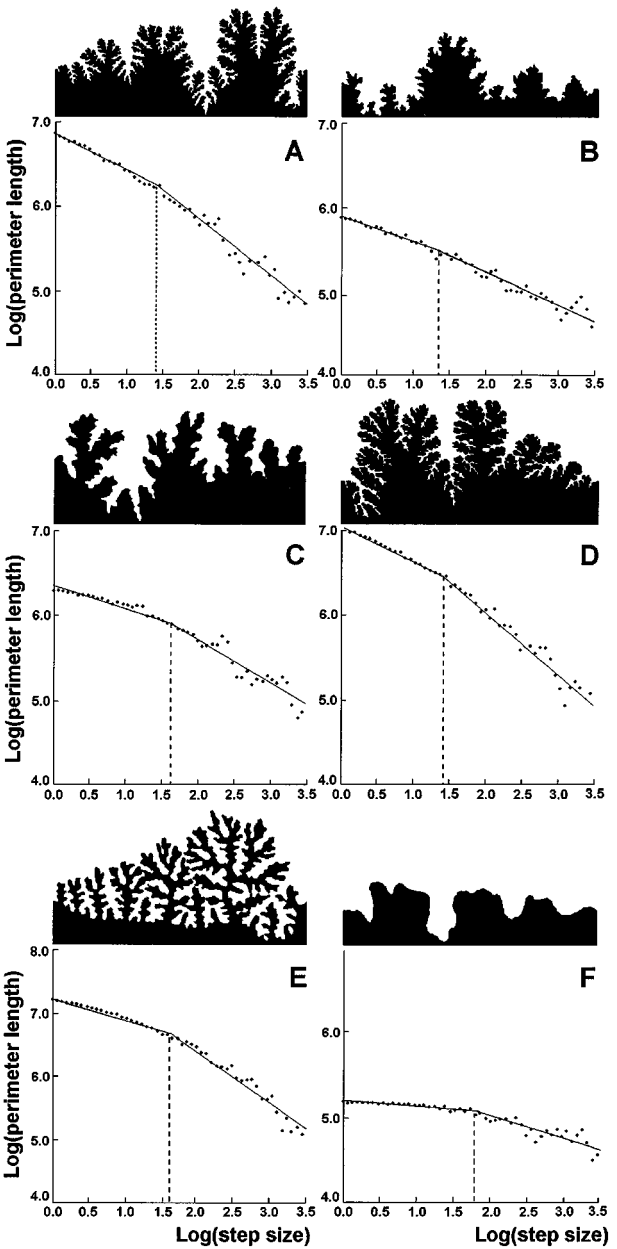

Figure 6. Inverse relation between the estimated perimeter and the rule length or step size in sutures of Late Jurassic ammonites. Note the cut-off point (X_c) calculated to distinguish between the fractal dimension at small (D_{f1}) and large (D_{f2}) scales.

dimensions in the two suture regions (i.e., below and beyond the cut-point, respectively), due to the variable degree of complexity presented. However, comparison of Figure 6(E) and (B), both having a small fractal dimension at low scales, shows that the former presents a sudden decrease in the slope, translated in a higher value of fractal dimension at large scales, which does not occur in the latter. The same effect is evident with higher fractal dimensions, as in the sutures shown in Figures 6(C) and (A). In this case, the value of D_{f2} for both sutures is around 1.6, but while suture complexity in Figure 6(C) is only visible at large-scales, which in Figure 6(A) is maintained at a small-scale, with a greater number of small folds being visible. Finally, the distinction between large- and small-scales of fractal dimension (and therefore suture complexity) is very useful to the description of these basic geometric aspects. This is shown in Figure 6(E), where the suture analyzed at a large-scale is so coiled that it almost fills a plane ($D_{f2} = 1.824$), but is comparatively simple at a small-scale. Clearly, there exists a wide angle between the curves characterizing the two regions. On the other hand, analysis of the suture illustrated in Figure 6(D), which also presents a high value of D_{f2}, shows that the complexity is maintained at all levels.

In conclusion, it can be argued that the distinction between such regions in fractal curves is not just of mathematical significance, but is also of geometric interest in terms of analyzing the fractal behavior of the sutures of ammonoid cephalopods, thus clarifying their interpretation. The method proposed in this paper characterizes, independently, two aspects of fractal objects: their complexity in terms of large and small suture details (estimated by means of D_{f2} and D_{f1}, respectively), and the degree of self-similarity that can be characterized by X_c.

ACKNOWLEDGMENTS

This research was supported in part by projects PB97-1082 (P. Palmqvist) and PB97-0803 (F. Olóriz), funded by DGESIT and SGPICYT. We gratefully acknowledge Richard A. Reyment, W. Bruce Saunders, and Cameron J. Tsujita for their insightful comments and helpful review of the original manuscript.

REFERENCES

Batt, R. J., 1991, Sutural amplitude of ammonite shells as a paleoenvironmental indicator: Lethaia, v. 24, no. 2, p. 219–225.

Bayer, U., 1985, Pattern recognition problems in geology and paleontology: Springer, Berlin, 229 p.

Bookstein, F. L., 1991, Morphometric tools for landmark data: Cambridge University Press, Cambridge, 435 p.

Boyajian, G. E., and Lutz, T., 1992, Evolution of biological complexity and its relation to taxonomic longevity in the Ammonoidea: Geology, v. 20, no. 11, p. 983–986.

Buckland, W., 1836, Geology and mineralogy considered with reference to natural theology, Vols. 1 and 2: Pickering, London, p. 599 and 128.

Canfield, D. J., and Anstey, R. L., 1981, Harmonic analysis of cephalopod suture paterns: Math. Geol., v. 13, no. 1, p. 23–35.

Cecca, F., 1992, Ammonite habitats in the Early Tithonian of Western Tethys: Lethaia, v. 25, no. 3, p. 257–267.

Damiani, G., 1986, Significato funzionale dell'evoluzione dei setti e delle linee di sutura dei nautiliodi e degli ammonoidi, *in* Pallini, G., ed., Atti I Convengo Internationale: Fossili, Evoluzione, Ambiente: Pergola, Roma, p. 123–130.

Daniel, T. L., Helmuth, B. S., Saunders, W. B., and Ward, P., 1997, Septal complexity in ammonoid cephalopods increased mechanical risk and limited depth: Paleobiology, v. 23, no. 4, p. 470–481.

Dommergues, J. L., Laurin, B., and Meister, C., 1996, Evolution of ammonoid morphospace during the Early Jurassic radiation: Paleobiology, v. 22, no. 2, p. 219–240.

Ebel, K., 1992, Mode of life and soft body shape in heteromorph ammonites: Lethaia, v. 25, no. 2, p. 179–193.

Fisher, D. C., 1986, Progress in organismal design, *in* Raup, D., and Jablonski, D., eds., Patterns and processes in the history of life: Springer, Berlin, p. 99–117.

García-Ruíz, J. M., Checa, A., and Rivas, P., 1990, On the origin of ammonoid sutures: Paleobiology, v. 16, no. 3, p. 349–354.

Gould, S. J., 1988, On replacing the idea of progress with an operational notion of directionality, *in* Nitecki, M. H., ed., Evolutionary progress: University of Chicago Press, Chicago, p. 319–338.

Henderson, R. A., 1984, A muscle attachment proposal for septal function in Mesozoic ammonites: Palaeontology, 27, no. 3, p. 461–486.

Hewitt, R. A., 1993, Relation of shell strength to evolution, *in* House, M. R., ed., The Ammonoidea: Environment, ecology and evolutionary change: Clarendon Press, Oxford, p. 35–56.

Hewitt, R. A., 1996, Architecture and strength of the ammonoid shell, *in* Landman, N. H., Tanabe, K., and Davis, R. A., eds., Ammonoid paleobiology: Plenum, New York, p. 297–343.

Hewitt, R. A., and Westermann, G. E. G., 1983, Mineralogy, structure and homology of ammonoid siphuncles: N. Jb. Geol. Paläont. Abh., v. 165, no. 3, p. 378–396.

Hewitt, R. A., and Westermann, G. E. G., 1986, Function of complexly fluted septa in ammonoid shells I. Mechanical principles and functional models: N. Jb. Geol. Paläont. Abh., v. 172, no. 1, p. 47–69.

Hewitt, R. A., and Westermann, G. E. G., 1987, Function of complexly fluted septa in ammonoid shells II. Septal evolution and conclusions: N. Jb. Geol. Paläont. Abh., v. 174, no. 2, p. 135–169.

Hewitt, R. A., and Westermann, G. E. G., 1988a, Stress and strain in *Nautilus* shells: Some limitations on the buoyancy control and vertical migration of ectocochliates, *in* Wiedmann, J., and Kullmann, J., eds., Cephalopods: Present and past: Schweizerbartsche, Stuttgart, p. 705–712.

Hewitt, R. A., and Westermann, G. E. G., 1988b, Buckling phenomena in cephalopod phragmocones and the muscle attachment proposal for septal function in Mesozoic ammonites: Hist. Biol., v. 1, no. 3/4, p. 225–231.

Hewitt, R. A., and Westermann, G. E. G., 1990, Mosasaur tooth marks on the ammonite *Placenticeras* from the Upper Cretaceous Bearpaw Formation of Alberta: Can. J. Earth Sci., v. 27, no. 3, p. 469–472.

Hewitt, R. A., and Westermann, G. E. G., 1997, Mechanical significance of ammonoid septa with complex sutures: Lethaia, v. 30, no. 3, p. 205–212.

House, M. R., and Senior, J. R., eds., 1981, The Ammonoidea: Systematics Association Special: Academic Press, London, Vol. 18, 593 p.

Jacobs, D. K., 1990, Sutural pattern and shell stress in *Baculites* with implications for other cephalopods shell morphologies: Paleobiology, v. 16, no. 3, p. 336–348.

Jacobs, D. K., 1996, Chambered cephalopod shells, buoyancy, structure and decoupling: History and red herrings: Palaios, v. 11, no. 6, p. 610–614.

Korn, D., 1992, Relationship between shell form, septal construction and suture line in Clymeniid cephalopods (Ammonoidea; Upper Devonian): N. Jb. Geol. Paläont. Abh., v. 185, no. 1, p. 115–130.

Kulicki, C., 1979, The ammonite shell: Its structure, development and biological significance: Palaeont. Pol., v. 39, no. 1, p. 79–142.

Kulicki, C., and Mutvei, H., 1988, Functional interpretation of ammonoid septa, *in* Pietronero, L., and Tosati, E., eds., Fractals in Physics: North-Holland, Amsterdam, p. 177–180.

Long, C. A., 1985, Intricate sutures as fractal curves: J. Morphol., v. 185, no. 3, p. 285–295.

Long, C. A., and Long, J. E., 1992, Fractal dimensions of cranial sutures and waveforms: Acta Anat., v. 145, no. 3, p. 201–206.

Lutz, T. M., and Boyajian, G. E., 1995, Fractal geometry of ammonoid sutures: Paleobiology, v. 21, no. 3, p. 329–342.

Mandelbrot, B., 1984, The fractal geometry of nature: Freeman, New York, 468 p.

McShea, D. W., 1991, Complexity and evolution: What everybody knows: Biol. Phil., v. 6, no. 3, p. 303–324.

Newell, N., 1949, Phyletic size increase, an important trend illustrated by fossil invertebrates: Evolution, v. 3, no. 1, p. 103–124.

Olóriz, F., and Palmqvist, P., 1995, Sutural complexity and bathymetry in ammonites: Fact or artifact?: Lethaia, v. 28, no. 2, p. 167–170.

Olóriz, F., Palmqvist, P., and Pérez-Claros, J. A., 1997, Shell features, main colonized environments, and fractal analysis of sutures in Late Jurassic ammonites: Lethaia, v. 30, no. 3, p. 191–204.

Olóriz, F., Palmqvist, P., and Pérez-Claros, J. A., 1999, Recent advances in morphometric approaches to covariation of shell features and the complexity of suture lines in Late Jurassic ammonites, with reference to the major environments colonized, *in* Olóriz, F., and Rodríguez-Tovar, F. J., eds., Advancing research on living and fossil cephalopods: Plenum, New York, p. 273–293.

Olóriz, F., Palmqvist, P., and Pérez-Claros, J. A., 2002, Morphostructural and taxonomic imprinting on sutural frilling in Late Jurassic ammonites: Lethaia, v. 35, in press.

Pfaff, E., 1911, Über Form und der Ammonitensepten und ihre Beziehungen zur Suturline: Jber. Nieder. Geol. Ver., v. 4, no. 1, p. 207–223.

Richardson, L. F., 1961, The problem of contiguity: An appendix of statistics of deadly quarrels: Gen. Syst. Yearbook, v. 6, no. 1, p. 139–187.

Saunders, W. B., 1995, The ammonoid suture problem: Relationships between shell and septum thickness and suture complexity in Paleozoic ammonoids: Paleobiology, v. 21, no. 3, p. 343–355.

Saunders, W. B., and Work, D. M., 1996, Shell morphology and suture complexity in Upper Carboniferous ammonoids: Paleobiology, v. 22, no. 2, p. 189–218.

Saunders, W. B., and Work, D. M., 1997, Evolution of shell morphology and suture complexity in Paleozoic prolecanitids, the rootstock of Mesozoic ammonoids: Paleobiology, v. 23, no. 3, p. 301–325.

Seilacher, A., 1975, Mechanische Simulation und funktionelle Evolution des Ammoniten-Septums: Paläont. Z., v. 49, no. 3, p. 268–286.

Seilacher, A., 1988, Why are nautiloid and ammonite sutures so different?: N. Jb. Geol. Paläont. Abh., v. 177, no. 1, p. 41–69.

Seilacher, A., and LaBarbera, M., 1995, Ammonites as cartesian divers: Palaios, v. 10, no. 6, p. 493–506.

Spath, L., 1919, Notes on ammonites: Geol. Mag., v. 56, no. 6, p. 27–35.

Stanley, S. M., 1973, An explanation of Cope's rule: Evolution, v. 27, no. 1, p. 1–26.

Ward, P. D., 1980, Function of cameral water in *Nautilus*: Paleobiology, v. 6, no. 2, 168–172.

Ward, P. D., 1987, The natural history of *Nautilus*: Allen and Unwin, London, 267 p.

Westermann, G. E. G., 1971, Form, structure and fuction of shell and siphuncle in coiled Mesozoic ammonoids: R. Ont. Mus., Life Sci. Contrib., v. 78, no. 1, p. 1–39.
Westermann, G. E. G., 1973, Strength of concave septa and depth limits of fossil cephalopods: Lethaia, v. 6, no. 4, p. 383–403.
Westermann, G. E. G., 1975, Model for origin, function and fabrication of fluted cephalopod septa: Paläont. Z., v. 49, no. 3, p. 235–253.
Westermann, G. E. G., 1977, Form and function of orthoconic cephalopod shell with concave septa: Paleobiology, v. 3, no. 3, p. 300–321.
Westermann, G. E. G., 1982, The connecting rings of *Nautilus* and Mesozoic ammonoids: Implications for ammonite bathymetry: Lethaia, v. 15, no. 3, p. 323–334.
Westermann, G. E. G., 1985, Post-mortem descent with septal implosion in Silurian nautiloids: Paläont. Z., v. 59, no. 1/2, p. 79–97.
Westermann, G. E. G., 1996, Ammonoid life and habitat, *in* Landman, N. H., Tanabe, K., and Davis, A., eds., Ammonoid paleobiology: Plenum, New York, p. 607–707.
Westermann, G. E. G., and Ward, P. D., 1980, Septum morphology and bathymetry in cephalopods: Paleobiology, v. 6, no. 1, p. 48–50.